

A Microfluidic System for Determining the Critical Shear Rate of Cells

Department of Bioengineering
Imperial College London

*A Year 3 Project Report Submitted in
Partial Fulfilment of the*

MEng Biomedical Engineering Degree

Supervisor: Professor James Moore Jr.

Department of Bioengineering
james.moore.jr@imperial.ac.uk

April, 2025

A Microfluidic System for Determining the Critical Shear Rate of Cells

Diego de la Esperanza, Mary Jebanesan, Jack Maeda,
Anish Mariathasan, Om Mahajan, Danny Shaw, Evan Zhang

Abstract

Cell therapies hold significant potential but are hindered by low cell viability, following injection through small-bore needles, which can be attributed to excessive shear rates. Currently, there is a lack of standardised data defining the critical shear rate thresholds different cell types can withstand. This project aimed to address this gap by developing and validating a microfluidic system capable of exposing cells to controlled shear rates relevant to clinical injections. Human Umbilical Vein Endothelial Cells (HUVECs) were exposed to a given shear rate within the device, and viability was assessed using a live/dead assay. Simulations informed the initial device design, which was subsequently validated using polystyrene microspheres and refined through iterative testing with HUVECs. Observations confirmed cells experienced high shear rates near channel walls, consistent with theoretical predictions. A statistically significant decrease in viability was observed between control HUVECs and those subjected to high shear rates within the device ($p=0.0004$), validating the system's capacity to induce shear-related cell death. Although challenges with achieving uniform cell distribution for clear imaging necessitated design modifications, this study establishes a validated platform for characterising the shear rate tolerance specific to different cell types. This work aims ultimately to inform the optimisation of syringe needle design to enhance the effectiveness and cost-efficiency of cell therapies.

1. Introduction

1.1. Background

Cell therapy represents a promising approach to treat a wide spectrum of diseases, from neurodegenerative disorders [1] to various cancers [2], by utilising living cells to repair, replace, regenerate or destroy damaged tissues [3]. Despite this clinical potential, a significant hurdle remains: ensuring high cell viability during administration [4]. Intravenous therapies often require injection through small-bore needles [5], a process which subjects cells to significant mechanical forces. Current post-injection viability rates can be as low as around 5% [4], meaning the majority of the cells are dead before being able to exert their intended therapeutic effects within the body. This necessitates multiple injections, escalating treatment costs by consuming valuable biological resources, thereby hindering the efficiency and widespread adoption of these promising therapies [6]. The primary cause of this low viability during injection has been a subject of investigation. Injected cells are notably sensitive to mechanical stress, and the forces experienced during syringe passage can induce mechanolysis [7].

Historically, shear stress was considered the main factor, as suggested by early studies exploring different suspension media. For example, Aguado et al. [8] observed improved viability in certain hydrogel carriers compared to standard saline solutions, initially linking viability to the medium's properties under extensional flow. However, they found that more viscous, cross-linked hydrogels (experiencing higher shear stress at constant flow rates) yielded higher viability which contradicted the shear stress hypothesis. More recent work has shown that excessive shear rate, rather than shear stress, is the critical factor responsible for cell damage during small-bore needle injections [9]. Shear rate refers to the rate of change of velocity at which adjacent layers of fluid move relative to each other.

Several approaches have been proposed to mitigate this damage. Hernández et al. [10] demonstrated that non-Newtonian polymer-nanoparticle hydrogels could significantly improve cell viability during injection. Using their hydrogel formulation, they increased the Human Umbilical Vein Endothelial Cells (HUVECs) viability from 68% in phosphate-buffered saline (PBS) to 88%. Their findings suggest that the shear-thinning properties of these materials create plug flow-like conditions which reduce the mechanical forces experienced by cells. However, these approaches introduce additional complexities, including substantially increased injection pressures (28 times higher than PBS) and potential compatibility issues with different cell types and therapeutic contexts [10]. While their findings

were based on empirical optimisation, there is a lack of quantitative data defining the maximum shear rates cells can withstand. This makes it difficult to rationally design hydrogels or syringe injection parameters for optimal viability across different cell types.

1.2. Project Overview

This project was designed to address this issue by determining standardised data which defines the threshold shear rates that different cell types can withstand before viability is compromised (the critical shear rate). This knowledge will contribute to optimising syringe and needle design [11], ultimately resulting in safer, more effective, and cost-efficient delivery of cell therapies by maximising the survival of administered cells.

However, pushing costly material through a syringe to assess the viability is not sustainable, as a significant amount of resources are consumed each time [6]. Instead, by using microfluidic devices, the amount of cell material required can be minimised while maintaining precise control over the conditions the cells experience.

Therefore, the aim of this project was to develop a microfluidic system to determine this critical shear rate for a given cell type.

1.3. Objectives

To achieve this aim, the following objectives were pursued:

1. Develop and validate a microfluidic device capable of exposing cells to a range of shear rates relevant to clinical injection scenarios.
2. Systematically expose HUVECs to varying shear rates within the microfluidic device.
3. Assess cell viability via a live/dead assay immediately following exposure.
4. Statistically analyse the viability data to identify and quantify the critical shear rate threshold for HUVECs, defining the point beyond which significant viability loss occurs.

2. Methods

2.1. Numerical Methods

Deciding the dimensions of the shearing region was the first stage of the design process. The device design are

introduced later in Figure 3. Microfluidic device fabrication produces rectangular channels [12, 13] with the highest precision. Therefore fluid flow in a rectangular duct was simulated using MATLAB (MathWorks, Natick, MA).

2.1.1. Optimisation of Calculations

Fluid flow in the shearing region was assumed to be Newtonian and fully developed [14], hence equation 1 [15] was used to determine the velocity profile in a rectangular duct.

$$u(y, z) = \frac{4h^2 \Delta P}{\pi^3 \mu L} \sum_{n=1,3,5,\dots}^{2N-1} \frac{1}{n^3} \left[1 - \frac{\cosh(\frac{n\pi y}{h})}{\cosh(\frac{n\pi w}{2h})} \right] \sin\left(\frac{n\pi z}{h}\right) \quad (1)$$

The equation involves a summation so the optimal number of terms was determined to balance computational accuracy and time.

2.1.2. Laminar Flow Check

The Reynolds number was calculated in order to ensure that flow would be laminar. Equation 2 was used to calculate the Reynolds number in a rectangular duct. Since velocities are dependent on the pressure difference, calculations were done for a range of pressure differences and different widths.

$$\text{Re} = \frac{\rho U D_h}{\mu} \quad (2)$$

where D_h is

$$D_h = \frac{2wh}{w+h} \quad (3)$$

2.1.3. Pressure Difference and Flow Rate Calculation

To obtain the shear rate from the velocity profile, the maximum gradient at the edges was calculated using the `gradient()` [16] function on MATLAB. A desired range of $20,000 \text{ s}^{-1}$ to $200,000 \text{ s}^{-1}$ shear rate was chosen [9] and the length of the shearing region was fixed at 1 cm. To accommodate cell diameters of $17 \mu\text{m}$, the height was fixed at $40 \mu\text{m}$. Varying the shearing region width and pressure drop would change the maximum shear experienced by the cells as they travel. Three widths of $40 \mu\text{m}$, $80 \mu\text{m}$ and $160 \mu\text{m}$ were chosen and

based on that, for varying pressure drops, the maximum shear rate was obtained.

The experimental setup as shown in Figure 1, uses syringe drivers which only accept flow rate as a parameter. Thus, equation 4 [15] was used to determine the flow rate for a given pressure drop and shearing region width.

$$Q = \frac{h^3 w \Delta P}{12\mu L} \left[1 - \sum_{n=1,3,5,\dots}^{2N} \frac{192h}{\pi^5 w n^5} \tanh\left(\frac{n\pi w}{2h}\right) \right] \quad (4)$$

2.2. Microfabrication

To fabricate the microfluidic devices, polydimethylsiloxane (PDMS, DOWSIL) was cast onto a 4-inch silicon wafer patterned with an SU-8 master mould. All patterns were made in SOLIDWORKS (Dassault Systèmes) and exported to KLayout [17] to create a design schematic for use in the soft lithography process.

Master moulds were fabricated by spin coating (WS-650MZ Modular) wafers in the photoresist SU-8-2075 and performing single-layer maskless photolithography (SP-UV) [18]. A 10:1 mixture of PDMS to curing agent (Sylgard 184 silicon elastomer) was degassed in a vacuum chamber, poured over the master mould to transfer the design to the PDMS and cured at 66°C for at least 2 hours [19]. Devices were then cut from the PDMS body, inlet and outlet holes were made with a biopsy punch, and the PDMS devices were bonded to coverslips with oxygen plasma treatment (Harrick PCD-002-CE).

2.3. Microsphere Preparation

Green fluorescent polystyrene microspheres (Cospheric, $R = 10\text{--}20 \mu\text{m}$) were used as model particles to validate simulated flow behaviour within the microfluidic device prior to cell-based experimentation. These microspheres were prepared to produce a concentration of approximately a million spheres per ml. To achieve this, approximately 10 mg of the microspheres was added to a 10 ml of PBS (ThermoFisher).

Due to the hydrophobic nature of polystyrene, a surfactant was added to the PBS solution to minimise the aggregation of the microspheres and ensure a uniform distribution in the solution. Despite this, cells may exhibit clustering, leading to uneven distributions. For these experiments 0.5 ml of dishwashing liquid (Fairy

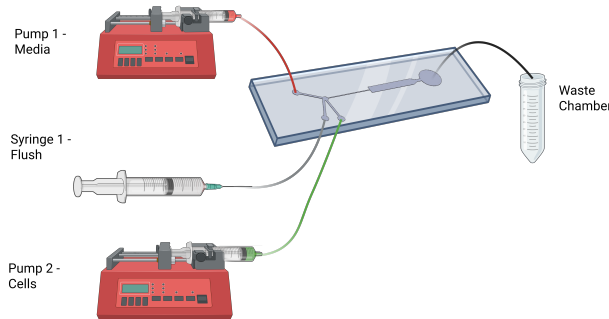


Figure 1: Schematic of the microfluidic system illustrating syringe pump connections for media, cell suspension, and flushing solution, and outlet configuration.

Liquid, Procter & Gamble) was added to minimise the clustering effect.

Samples were excited using a 488nm laser at 10% intensity and emission was collected between 520nm–550nm. The fluorescence microscopy was carried out on a Leica SP5 confocal microscope (Leica Microsystems, Wetzlar, Germany).

2.4. Experimental Setup

Prior to introducing cells, the system underwent rigorous preparation to remove debris and air bubbles, which would significantly disrupt flow and experimental results. The microfluidic device, mounted on the microscope stage, was inspected visually through the microscope. PBS was then manually pushed through the device using a standard plastic syringe to flush the channels and displace trapped air, with the excess fluid being driven into the waste chamber. Any trapped air bubbles and debris observed within the microstructure were dislodged and removed by this manual flushing process while under microscopic observation. Concurrently, the connecting tubing lines were inspected for bubbles and debris and flushed with PBS as necessary, until it was confirmed that the entire fluid path from the syringe to the outlet was free of air. This setup is illustrated in Figure 1.

Flow Rates

In order to subject the particles and cells to the desired shear rates within the shearing region of the microfluidic device, specific volumetric flow rates were calculated and applied using syringe pumps. The required flow rate depended directly on the target maximum shear rate ($\dot{\gamma}_{max}$), the channel geometry (width w , height h), and the viscosity (μ) of the fluid being

injected. The specific parameters for each experimental set are detailed in Table 1, where the viscosity was constant throughout at $\mu = 1.0 \text{ mPa} \cdot \text{s}$.

Apart from the final design, a syringe pump was connected to the secondary outlet to facilitate selective withdrawal of the cells. This was set to withdraw rate equal to 70% of the media inlet flow. The remaining fluid volume (30%) exited the device through the primary outlet, which functioned as the waste outlet.

2.5. Cell Preparation

2.5.1. Aseptic Preparation

To create the aseptic conditions appropriate for working with cells, all surfaces of a Class II, Type A biosafety cabinet [20] were disinfected with 70% ethanol and allowed to dry before introducing sterile reagents and equipment [21]. All reagents and equipment were sprayed with 70% ethanol prior to moving into the cabinet [22]. Appropriate personal protective equipment (PPE), including a laboratory coat and sterile gloves were worn throughout. All procedures were conducted under sterile conditions within the biosafety cabinet to minimise contamination risk.

2.5.2. Cell Culture

HUVECs were chosen to compare results to Aguado et al. [8]. The HUVECs (ThermoFisher) were cultured in media, composed of 500 mL Endothelial Cell Growth Medium 2 (PromoCell), 27 mL Endothelial Cell Growth Medium MV 2- (PromoCell), and 5 mL Penicillin-Streptomycin (ThermoFisher) [23]. Cells were maintained in a humidified incubator at 37 °C with 5% CO₂ [20].

For routine passaging, cells were detached upon reaching 70–90% confluence. Spent medium was aspirated, and the monolayer was washed 3 times with PBS to remove residual serum [24]. Trypsin-EDTA solution (0.025% – 0.05%) (ThermoFisher) was added at a volume equivalent to one-tenth of the flask surface area and incubated at room temperature until detachment was confirmed microscopically [20]. Trypsin activity was neutralised by adding double the volume of HUVEC media, which acted as a trypsin inhibitor solution. The cell suspension was centrifuged at 180 g for seven minutes [20]. The resulting cell pellet was resuspended in fresh, pre-warmed complete growth media and seeded into new flasks.

Experiment Type	Particles/Cells	Channel W×H (μm)	Target $\dot{\gamma}_{max}$ (s ⁻¹)	Calculated Flow Rate, Q (μL min ⁻¹)
Initial Design	Polystyrene	160 × 40	50 000	211.0
Intermediary Designs	HUVECs	160 × 40	50 000	211.0
Current Design	HUVECs	160 × 40	100 000	304.0

Table 1: Experimental flow parameters for different test conditions in the microfluidic device. The shearing channel length was 1 cm for all experiments listed.

2.5.3. Imaging Preparation

Cells designated for live/dead assay staining were prepared in accordance with standard passaging procedures. Following detachment with trypsin-EDTA and neutralisation with medium, cells were resuspended in Minimum Essential Medium (MEM) (ThermoFisher) at a concentration of 2×10^6 cells/mL.

A live/dead assay solution was prepared by mixing 10 μL of Ethidium Homodimer-1 solution with 5 mL of PBS, followed by the addition of 2.5 μL of Calcein AM [25]. This solution was vortexed thoroughly and protected from light with aluminium foil throughout the preparation and incubation process [26]. The prepared staining solution was added to the cell suspension in a 1:1 ratio, and the mixture was reverse pipetted to ensure uniform staining. The suspension was incubated at room temperature for 30 minutes in the dark. [25].

Following incubation, 1 mL aliquots of the stained cell suspension were transferred into Eppendorf tubes for imaging. A control sample was prepared by treating cells with 70 % ethanol to induce complete cell death. Fluorescence microscopy was performed under dark conditions to prevent photobleaching. Three sets of images, each consisting of red (Ethidium Homodimer-1) and green (Calcein AM) channels, were captured for three distinct regions per sample to ensure representative data collection.

2.6. Determination of Cell Viability

Cells were classified into three states: live, dead and ‘damaged’. Given that most ‘damaged’ cells die within 24 hours post-injection [27], a binary classification of live or dead was adopted for the purposes of this project. The viability was assessed using a standard live/dead assay with Calcein AM and Ethidium Homodimer-1.

This combination was used for the compatibility of both dyes, enabling the simultaneous assessment of the live and dead populations [28]. In addition to this, the assay was fixation free, which allowed for non-destructive assessment of cell viability and ensured that

cellular activity was preserved throughout the experiment. Additionally, the assay enabled an immediate viability measurement while the cells remained in the microfluidic environment, streamlining the experiment workflow.

Samples were excited using a 488 nm laser at a 20 % intensity, with the fluorescence emissions of the Calcein AM and Ethidium Homodimer-1 acquired at 530 ± 12 nm and 645 ± 20 nm respectively [29]. Fluorescence microscopy was carried out on the Leica SP5 confocal microscope. Cells exhibiting purely green or red fluorescence were classified as live or dead, respectively. Cells exhibiting both green and red fluorescence were classified as ‘damaged’, and therefore included within the dead cell population.

Cell viability was calculated with the following equation:

$$\text{Cell Viability (\%)} = \left(\frac{\text{Number of Live Cells}}{\text{Total Number of Cells}} \right) \times 100\% \quad (5)$$

2.7. Statistical Analysis

A statistical analysis was performed to compare the mean cell viability between the control and output groups. The central limit theorem enables the assumption that the data will tend towards a normal distribution [30]. Based on this assumption, a two-sample unpaired t-test (Appendix B) was selected as the appropriate statistical test. The null hypothesis states that the means of the two samples are equal, while the alternative hypothesis states there is a statistically significant difference between them. For the purposes of this project, a significance level of $\alpha = 0.05$ was adopted.

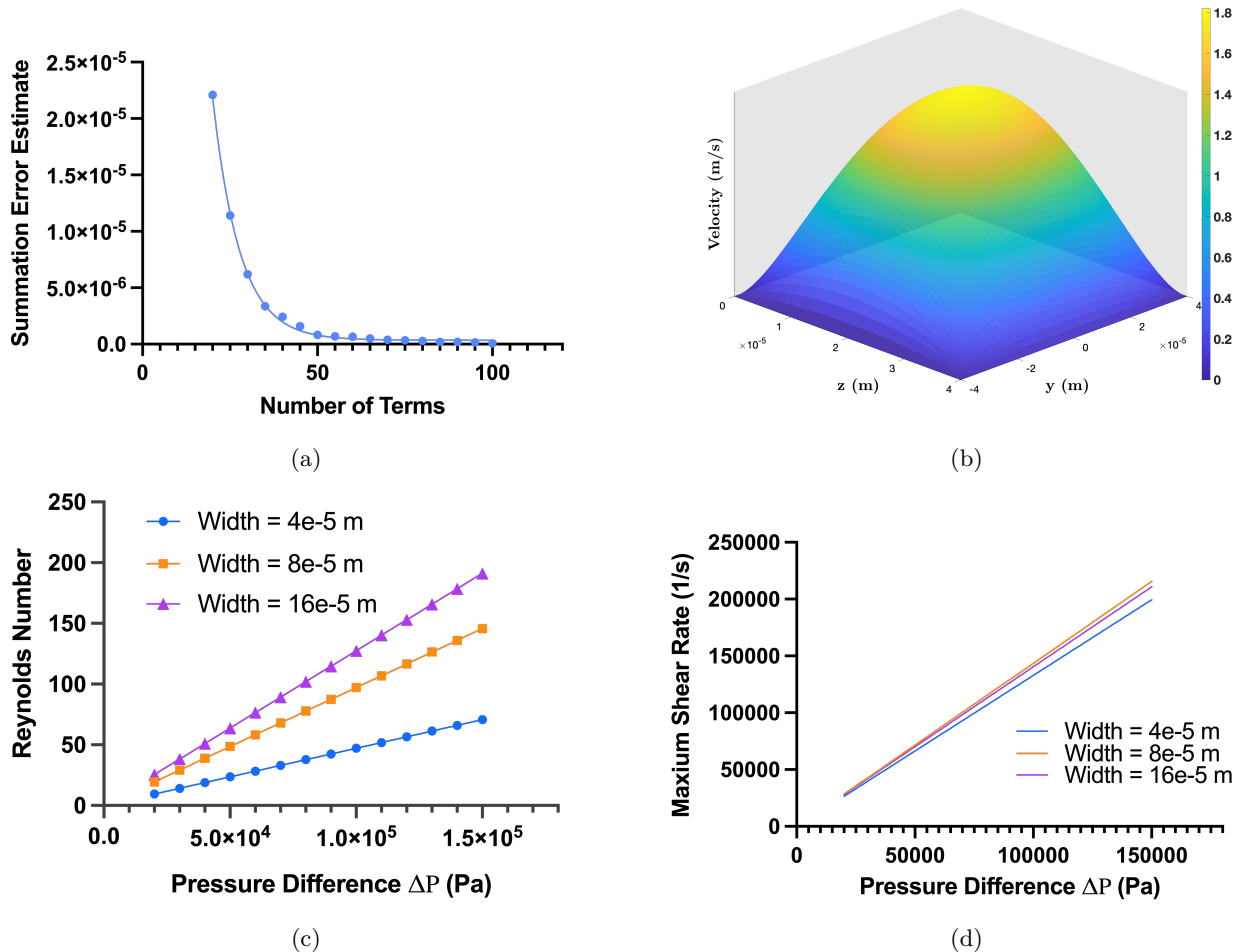


Figure 2: Numerical simulations for flow in a rectangular channel. (a) Convergence of the velocity profile with increasing number of terms based on equation 1. (b) Velocity profile for fully developed laminar flow in a rectangular duct. (c) Variation of Reynolds number in the shear region with increasing pressure difference and different channel widths. (d) Effect of pressure difference and channel width on the maximum shear rate at the wall edge.

3. Results

3.1. Numerical Simulation

Equation 1 was summed from 20 to 100 terms with increments of 5, and the maximum difference from the previous calculation was plotted in Figure 2a. It is to be noted that although the computational time increased as number of terms calculated increased, the time and computing resources were insignificant and did not affect the project.

Based on varying shear region widths, velocity profiles were generated as shown in Figure 2b, and these were used to determine the pressure drop necessary to achieve the desired shear rate.

From equation 2, the Reynolds number was calculated and plotted as shown in Figure 2c. The Reynolds

number increased from about 20 to 200 over the increasing pressure differences of 20,000 Pa to 150,000 Pa. The Reynolds number was calculated for the different channel widths.

3.2. Initial Design

3.2.1. Device Geometry

The first design of the microfluidic device had a channel height of $40 \mu\text{m}$ and incorporated three inlets (A, B, C in Fig. 3a) to supply the device with media, PBS, and HUVECs separately. The inlets converged into a constriction region $160 \mu\text{m}$ wide and 1 cm in length (H in Table 2), which was followed by a 1:5 gradual expansion to primary and secondary outlets (O, P in Fig. 3a).

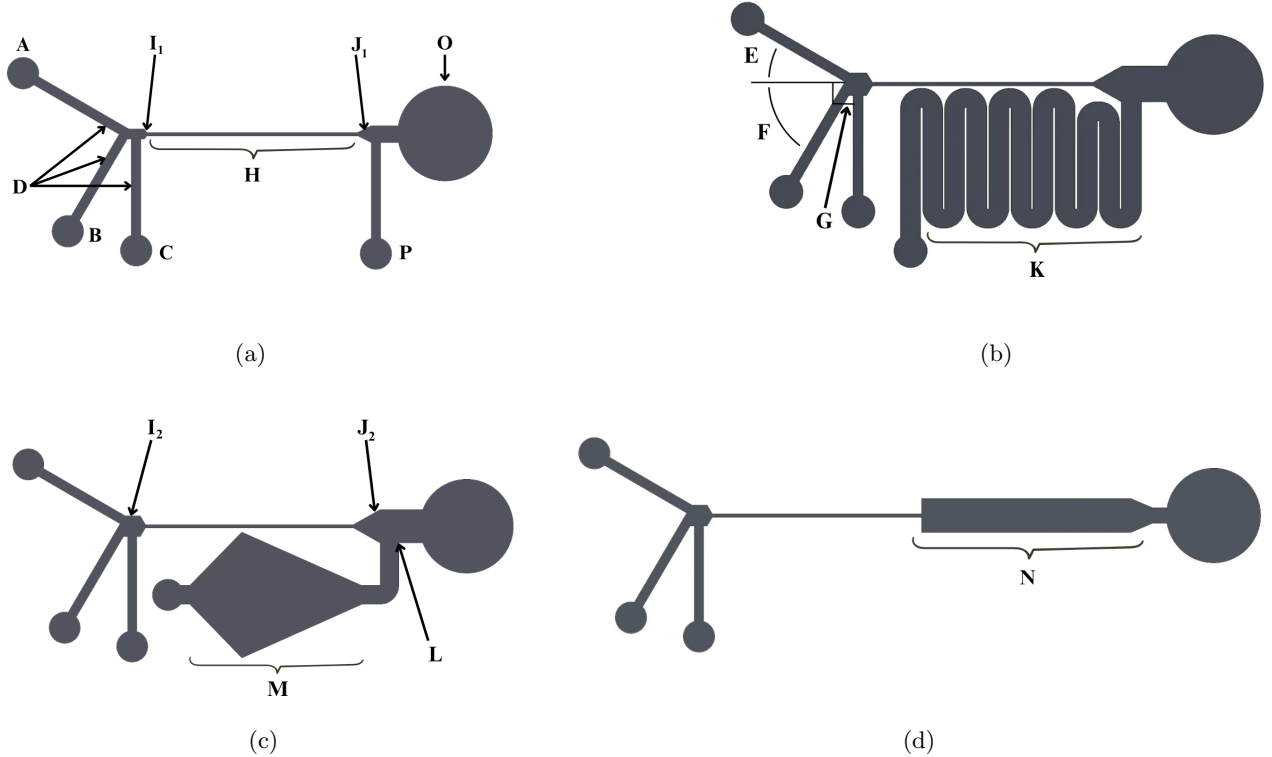


Figure 3: Evolution of microfluidic device design, progressing from (a) the initial concept to (b) a serpentine channel, (c) a kite expansion, and (d) a rectangular expansion. Refer to Table 2 for Feature Names and Dimensions.

Label	Feature Name	Dimensions	Relevant Design(s)
A	Media Inlet	Diameter: 1.5 mm	All
B	Cell Inlet	Diameter: 1.5 mm	All
C	Flushing Inlet	Diameter: 1.5 mm	All
D	Inlet Channels (All)	L: 4500 μm , W: 450 μm , H: 40 μm	All
E	Media Inlet Angle	30°	All
F	Flushing Inlet Angle	60°	All
G	Cell Inlet Angle	90°	All
H	Shearing Region	L: 1 cm, W: 160 μm , H: 40 μm	All
I ₁	Shearing Region Entrance	L: 120 μm , W: 210 μm , H: 40 μm	a
I ₂	Shearing Region Entrance	L: 240 μm , W: 420 μm , H: 40 μm	b, c, d
J ₁	Shearing Region Exit	L: 360 μm , W: 640 μm , H: 40 μm	a
J ₂	Shearing Region Exit	L: 720 μm , W: 1280 μm , H: 40 μm	b, c, d
K	Serpentine Structure	Effective L: 65 500 μm , W: 40 μm H: 40 μm , Turn Radius: 900 μm	b
L	Kite Structure - Neck	W: 900 μm	c
M	Kite Structure - Expansion	W: 6020 μm	c
N	Rectangle Structure - Expansion	W: 1600 μm , L: 10 000 μm	d
O	Primary Outlet	Port Diameter: 4.5 mm	All
P	Secondary Outlet	Port Diameter: 1.5 mm	a, b, c

Table 2: Dimensions of key features for each microfluidic device configuration (a-d). Refer to Figure 3 for location of features on the microfluidic device.

3.2.2. Microsphere Imaging

Figure 4 demonstrates the distinct particle distribution patterns in three key regions within the device: the inlet region (Fig. 4a), the shearing region (Fig. 4b) and the outlet region (Fig. 4c).

Within the inlet region, the microspheres adhered predominantly along the bottom edge of the channel, from the cell inlet channel to the entrance of the shearing region. As the microspheres entered the shearing region, they remained towards the left side of the region, forming a boundary layer approximately 20–70 μm from the left side of the wall. Upon reaching the outlet region most microspheres were withdrawn through the collection channel, now adhering towards the upper side of the channel. This result was repeated across multiple experimental runs, confirming the behaviour of the spheres within the device.

3.3. Intermediary Designs

3.3.1. Device Geometry

Two secondary designs were developed following the previous observations. In both designs, the shear-zone entrance and exit were scaled up twofold, resulting in a 1:10 gradual expansion at the exit. The width of both secondary outlet channels was increased from 0.45 mm to 0.9 mm , and the secondary outlet was modified to include a serpentine channel (Fig. 3b) or a kite geometry (Fig. 3c), with an expansion ratio of 1:6.5.

3.3.2. Cell Imaging

The flow behaviour of HUVECs was illustrated across 5 key regions within the new device: inlet region (Fig. 5a and Fig. 5b), outlet region (Fig. 5c), entrance to kite region (Fig. 5d), middle of the kite region (Fig. 5e), and upper kite region with a section of the shearing region (Fig. 5f). Although cell density was significantly lower compared to the polystyrene microsphere experiments (Fig. 4), HUVECs exhibited similar flow patterns with strong wall adhesion throughout the device. Within the kite region (Fig. 5d-5f), cells predominantly adhered to the right wall of the expansion area. In particular, few cells were observed to break away from this boundary to occupy the central area of the kite region.

The images obtained from the primary expansion region revealed a considerable concentration of cells within this area (Fig. 6a-6c). These cells exhibited minimal movement, remaining essentially stationary, allowing clear images to be obtained of this region. The

bright-field image (Fig. 6a) confirms the density and distribution of cells within this region. Comparison of the fluorescence seen in Fig. 6b (green fluorescence) and Fig. 6c (red fluorescence) enables the determination of cell viability within this population.

3.3.3. Cell Viabilities

Table 3 shows the results from these experiments. A two-sample unpaired t-test reveals that the means of the control group ($n=15$, $M = 6.07$, $SD = 4.48$) and the output group ($n = 11$, $M = 0.77$, $SD = 0.89$) are statistically different. The resultant test statistic was $t(15.49) = 4.46$, which results in $p = 0.0004$. The mean difference between the two groups was 5.30 (95 % CI [2.77, 7.82]), suggesting that the mean of the control group was statistically higher at a significance level of $\alpha = 0.05$.

3.4. Current Design

3.4.1. Device Geometry

Following secondary experiments, subsequent designs (Fig. 3c and 3d) were derived from serpentine and kite-shaped geometries. In this iteration, the secondary outlet was removed and the primary outlet channel was modified into a 1:10 rectangular expansion.

4. Discussion

This project set out to develop a system by which we could determine the critical shear rate for a given cell type. This goal was achieved via the creation of a microfluidic device, the design of which was refined over several iterations in order to better fulfill its primary purpose. Successful verification of the device's primary function occurred via the passage of assay-stained cells through the device and subsequent imaging.

4.1. Numerical Simulations

From Figure 2a, it can be observed that the error plot converges towards zero as the number of terms increases. After approximately $n = 50$ terms, there were negligible changes in the solution, indicating that convergence had been effectively achieved. Consequently, to balance computational efficiency with accuracy, the number of terms used to simulate the flow was set at 50.

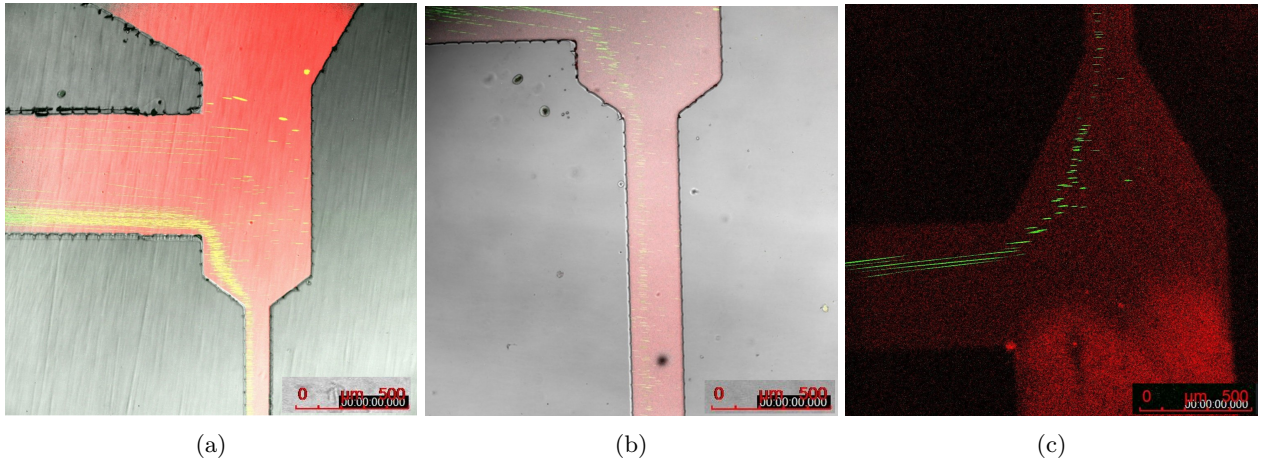


Figure 4: Flow behaviour of polystyrene microspheres (green fluorescence) in the device across 3 key regions: (a) inlet region (Label I₁), (b) inlet/shearing region (Label H/I₁), (c) outlet region (Label J₁). As it can be seen, across all regions, cells strongly adhere to the edges of the device. All labels are in reference to 3.

The Reynolds number remained relatively low ($Re < 200$) for all channel widths and range of pressure differences (Fig 2c). It is widely accepted that the Reynolds number for flow in microfluidics is often less than 1 [31], which seemed contradictory to the results obtained. However, it was concluded that this deviation from the commonly reported range could be explained by the much higher pressure differences used in the device [32, 33].

However, an excessively high pressure gradient could lead the microfluidic device to shatter, potentially damaging the microscope. To achieve higher shear rates without increasing the pressure drop, microfluidic devices featuring a region of variable width were used. This is illustrated in Figure 2d, where, for identical pressure drops, the device with different width produced a different shear rate.

Furthermore, the pressure drop and flow rate are directly proportional, as demonstrated by equation 4. Consequently, by regulating the pressure difference, the flow rate was effectively controlled, thereby reducing the volume of media and cellular material required to obtain the results.

4.2. Initial Design

4.2.1. Device Geometry

The initial prototype was designed to use polystyrene microspheres to validate the behaviour of cells. At this point, concerns regarding viability assessment were yet to be considered. All the designs aimed to have the cells experience the maximum shear rate at the edges of the channel, given the steepest velocity gradient occurs in

close proximity to the channel walls (Fig. 2b). The shear zone was sufficiently narrow to achieve this while remaining wide enough to reduce cell aggregation and thus mitigate the risk of blockage.

The device design incorporated separate inlets for culture media (A in Fig. 3) and the cell suspension (B in Fig. 3), enabling the injection of media at flow rates significantly greater than that of the cell suspension. This substantially reduced the consumption of valuable cellular resources by allowing cell introduction at a lower flow rate. However, despite the cells being at a lower flow rate, they were accelerated upon joining the faster-moving media stream, such that they still experienced the high shear rate desired at the channel walls. Theoretical predictions confirmed the microfluidic system operated at a low Reynolds number (Fig. 2c), signifying laminar flow where viscous forces dominate over inertial forces. Consequently, convective mixing of cells across streamlines was minimal. As such, the cells remained confined to the lower region of the channel, specifically adjacent to the bottom wall.

As a result of the shear region constriction, cells experienced a local acceleration and so a downstream expansion was incorporated at the shear zone exit to decelerate the cells, such that they could be manipulated as desired. This was done by increasing the cross-sectional area through which they flow, which is a feature reflected across all designs. The length of the shear region was carefully chosen to provide enough exposure time to the shear rate, enabling the observation of changes in cell viability without unnecessarily increasing the size of the device.

Due to the risk of debris and bubbles within the microfluidic device, an extra inlet intended as a "flushing" inlet was incorporated (C in Fig. 3). This en-

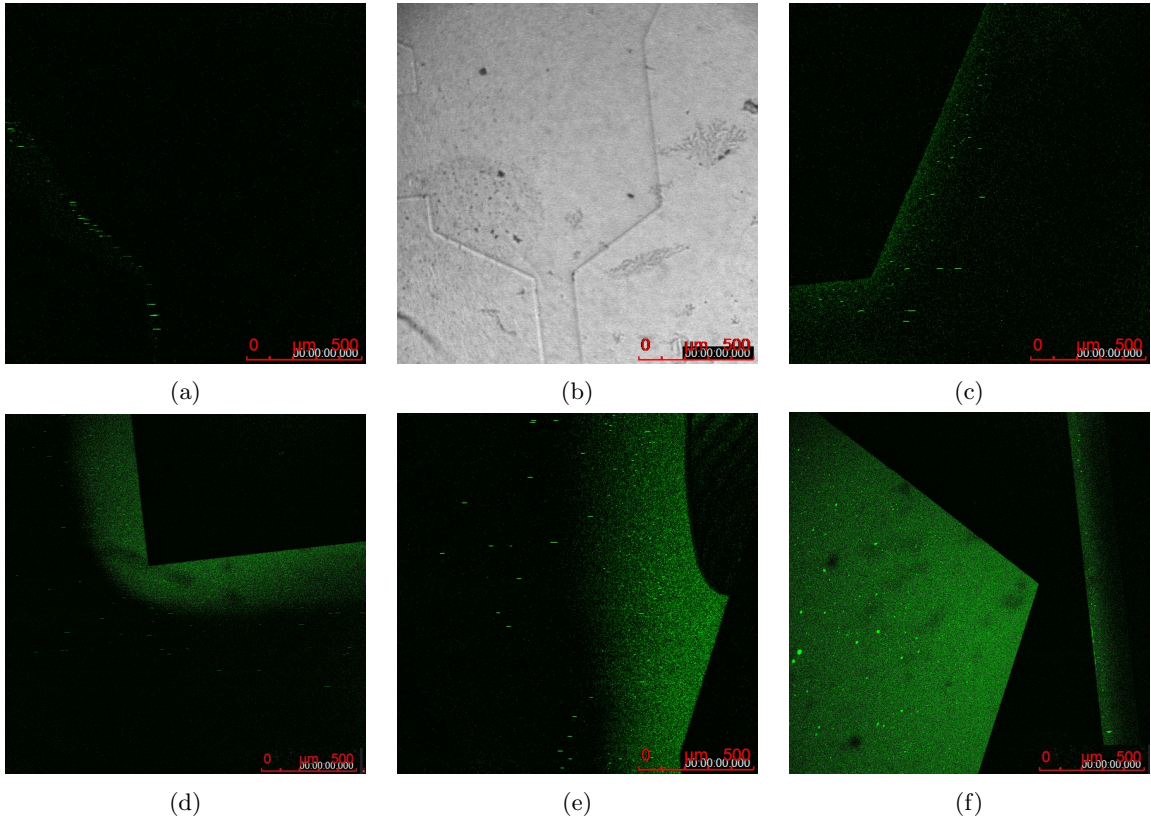


Figure 5: Flow behaviour of HUVECs illustrated across 5 key regions in the microfluidic device: (a) and (b) inlet region in green fluorescence and bright field respectively (Label I_2), (c) outlet region (Label J_2), (d) entrance to kite region (Label L), (e) middle of the kite region (Label M), and (f) upper kite region with a section of the shearing region (Label M). All labels are in reference to Figure 3.

sured the clearance of channels prior to the injection of polystyrene spheres/cells, enabling the smooth-running of experiments.

Following the expansion region, the microchannel bifurcated into two distinct outlets, designated as the primary and secondary outlets (O, P in Table 2). The secondary outlet was intentionally designed for the collection of cells intended for viability assessments. To facilitate this selective withdrawal, a syringe pump connected to the secondary outlet operated at a constant withdrawal rate equal to 70 % of the total inlet media flow rate. It should be noted that the remaining fluid volume exited the device through the primary outlet, which was implemented to function as the waste outlet.

firm the predicted flow patterns prior to subsequent cell-based experimentation.

Results indicated a consistent localisation of polystyrene microspheres immediately adjacent to the channel boundaries and shearing region, as illustrated in Figures 4b and 4c. This observation was consistent with our design goals, and showed the minimal lateral migration of the cells as intended.

In summary, this device prototype with polystyrene microspheres provided a valuable insight into the expected behaviour of cells within the device. However, it would be unsuitable to use for viability assessments as this requires the slowing down and spreading out of cells for clear imaging.

4.2.2. Microsphere Image

Figure 4a shows the polystyrene microspheres used to validate the functionality of the microfluidic device and to characterise the flow behaviour under controlled conditions. These microspheres were selected due to their size similarity to HUVECs, enabling an assessment of cell-like behaviour within the microchannels. The aim of this preliminary experiment was to con-

4.3. Intermediary Designs

4.3.1. Device Geometry

For subsequent experiments utilising cells instead of polystyrene microspheres, two microfluidic device designs incorporated modifications aimed at potentially enabling post-shear viability imaging.

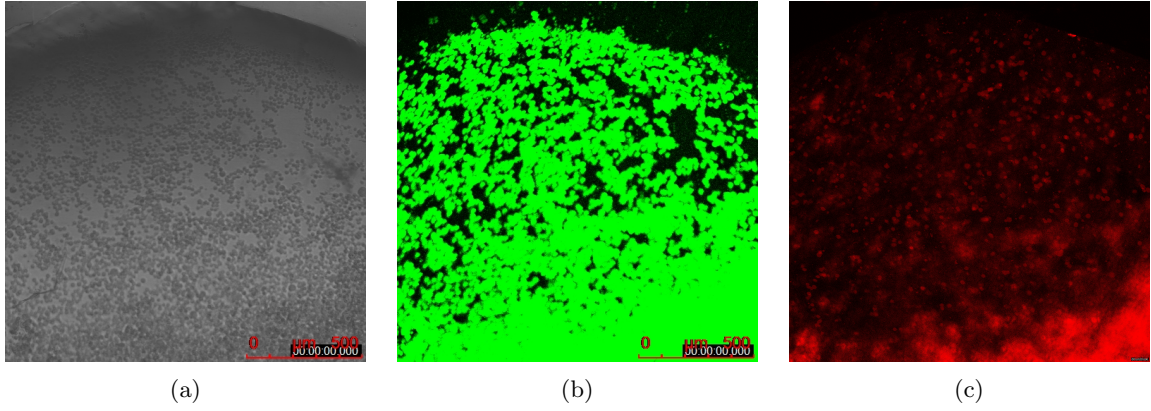


Figure 6: HUVEC accumulation and viability in the primary expansion zone post-experimentation (Label O in Fig. 3). (a) Bright-field image. (b) Live cells (green fluorescence, Calcein AM). (c) Dead cells (red fluorescence, Ethidium Homodimer-1).

The likelihood of capturing clear images of cells is greater at lower velocities. Furthermore, spreading cells more evenly across the channel width ensures the captured sample is more representative of the total population, as it increases the number of cells visible in the field of view. This leads to higher accuracy in viability calculations and so several design features were implemented to achieve this.

Firstly, the shear zone exit was widened (J_2 in 3c). This increase in cross-sectional area reduces fluid velocity due to mass conservation, thereby slowing the cells and encouraging their dispersion.

Secondly, distinct downstream structures were integrated into the two prototypes to prepare cells for imaging: the design in 3c included a kite-shaped expansion region (M) utilising mass conservation to decelerate and spread cells laterally, whereas the design in 3b incorporated a serpentine channel (K) to induce mixing across streamlines for cell distribution homogenisation.

A major issue that repeatedly occurred in previous experiments was the blockage of the inlet and outlet channels due to factors such as debris, bubbles, or the build-up of microspheres. Despite implementation of the flushing inlet, it was often insufficient in the removal of these issues. In response to this, the entrance, exit and secondary outlet size was doubled to minimise future complications.

4.3.2. Cell Imaging

The imaging results for the "kite" design had some limitations. As expected, cells adhered to the lower edge of the shearing region, confirming the consistent exposure to the highest shear rates. However, when cells passed to the kite-expanded region, most cells didn't spread out as intended. The majority adhered to the

upper wall of the kite-region and only a few dispersed into the central area. This tendency of cells to remain at the top of the kite resulted in dense clustering within a limited area, making it difficult to capture a sufficient number of clear cells in a single frame. As a result, the percentage of cell viability is less representative.

4.3.3. Cell Viabilities

A primary objective of this project was to create a device capable of simulating the different shear rates experienced by cells during passage through small-bore needles and to assess the resulting impact on cell viability. The comparison between the control ($M = 6.07\%$) and output ($M = 0.77\%$) groups revealed a statistically significant difference ($p = 0.0004$), confirming the device's ability to expose the cells to shear rates exceeding that of their threshold. Despite the unexpectedly low baseline viability observed in control groups, this clear statistical distinction strongly corroborates the fundamental premise that shear rates generated within the device significantly impact cell survival.

Low viability values in the control and high variance in the control group ($SD = 4.48$) are mainly attributed to suboptimal protocol timing, specifically delay in post-assay evaluation. During the experimental time-frame, cells experienced prolonged exposure to the Calcein AM/Ethidium Homodimer-1 assay outside of ideal culture conditions. This led to progressive membrane compromise and cytotoxicity, thereby artificially lowering the measured viability over time [34]. A similar effect would have impacted the output viability. Despite this, the data strongly indicates that the shear conditions simulated by the device impose a significant, detrimental impact on HUVECs viability. This validates the device's capability to function as intended for investigating these shear-dependent cellular responses.

Experiment Group	Alive Cells	Dead/Damaged Cells	Total Cells	Viability (%)
Control 1	24	154	178	13.48
	9	364	373	2.41
	5	216	221	2.26
	6	284	290	2.07
	14	183	197	7.11
	33	407	440	7.50
Control 2	2	45	47	4.26
	5	106	111	4.50
	18	98	116	15.52
	2	35	37	5.41
	6	39	45	13.33
	8	121	129	6.20
Control 3	4	82	86	4.65
	5	229	234	2.14
	1	422	423	0.24
Output 1	1	105	106	0.94
	2	105	107	1.87
	3	182	185	1.62
	4	196	200	2.00
Output 2	0	88	88	0.00
	3	141	144	2.08
	0	101	101	0.00
Output 3	0	81	81	0.00
	0	76	76	0.00
	0	118	118	0.00
	0	101	101	0.00
Average (Controls)	—	—	—	6.07
Average (Outputs)	—	—	—	0.77

Table 3: Summary of cell viability counts for control and output experiments.

4.4. Current Design

Given the cells in the previous "kite" geometry did not spread out sufficiently within the observation area, a third iteration of the design was implemented. The wider rectangular expansion zone creates an abrupt increase in cross-sectional area at the entrance to the expansion zone, resulting in a decrease in the average linear fluid velocity to conserve mass flow rate. Concurrently, the laminar flow streamlines diverge laterally to occupy the increased channel width. This combination of reduced velocity and streamline divergence significantly increases the transit time and the average spacing between adjacent cells, thereby mitigating the interactions that lead to aggregation. Ultimately, this revised geometry aimed to give a clearer visualisation of spatially separated, individual cells, in order to better assess viability.

5. Conclusion

This project successfully developed and iteratively refined a microfluidic system to investigate the impact of shear rate on cell viability during injection-like conditions. The system was validated using simulations, polystyrene microspheres, and experiments with HU-

VECs. HUVECs were exposed to controlled shear rates, and cell viability was assessed using fluorescence microscopy, which revealed a statistically significant difference in values when compared to controls, thereby confirming the system's ability to induce shear-related viability loss. Key observations included the tendency of cells to adhere to channel walls, experiencing the highest shear rates, consistent with laminar flow predictions. However, achieving uniform cell dispersal for clear viability imaging in the downstream expansion zones proved challenging, leading to multiple design iterations incorporating features such as kite-shaped geometry and wider rectangular expansions.

While the system demonstrated the capability to apply controlled shear, limitations included testing only HUVECs and difficulties in obtaining precise viability quantification due to cell clustering. Additionally, HUVECs were not systematically exposed to varying shear rates as initially intended, meaning a critical shear rate threshold could not be calculated.

The microfluidic device developed in this study provides a useful tool for determining the critical shear rate that different cell types can tolerate. The findings lay a strong foundation for future experiments aimed at developing a generalised dataset of critical shear rates for various cell types.

6. Future Work

Several limitations identified in this study necessitate further investigation to enhance the accuracy, applicability, and overall impact of the findings.

The scope should be expanded to investigate other cell types commonly employed in needle-based therapies. Given that different cells exhibit varying mechanical sensitivities and critical shear thresholds [35], characterising these specific responses is crucial. Determining the differing critical shear rates will provide essential data for optimising syringe design for a range of cell types.

It would also be desirable to incorporate multiple channels with distinct geometries onto a single device. This parallel processing capability would allow simultaneous exposure to different shear rates, greatly accelerating data acquisition and saving experimental time.

Ultimately, this research aims to generate quantitative data on cell-specific shear tolerance. Such data can directly inform the rational design of improved clinical injection systems, including needles and catheters [36, 37], to minimise cell damage during administration. Maximising the viability of delivered cells will enhance the success rates of cell therapies, reduce patient treatment costs, and help expand the therapeutic potential of these advanced treatments for many challenging diseases around the world.

References

- [1] Farzaneh Sivandzade and Luca Cucullo. Regenerative stem cell therapy for neurodegenerative diseases: An overview. *International Journal of Molecular Sciences*, 22(4):2153, Feb 2021.
- [2] Prateek Dabas and Anish Danda. Revolutionizing cancer treatment: a comprehensive review of cart cell therapy. *Medical Oncology*, 40(9):275, Aug 2023.
- [3] Kunal D. Sutar, Rutika D. Harshad, Omkar S. Sangar, Aishwarya C. Patil, and Santosh A. Payghan. An overview of stem cell therapy. *Research Journal of Topical and Cosmetic Sciences*, 13(1):21–26, 2022.
- [4] Mahetab H. Amer, Felicity R. A. J. Rose, Kevin M. Shakesheff, Michel Modo, and Lisa J. White. Translational considerations in injectable cell-based therapeutics for neurological applications: concepts, progress and challenges. *npj Regenerative Medicine*, 2:23, 2017.
- [5] Mahendra K. Mamidi, Gopal Singh, Jamuna M. Husin, Koshy G. Nathan, Gopinath Sasidharan, Zubaidah Zakaria, Raghavan Bhonde, Anish S. Majumdar, and Anish K. Das. Impact of passing mesenchymal stem cells through smaller bore size needles for subsequent use in patients for clinical or cosmetic indications. *Journal of Translational Medicine*, 10:229, Nov 2012.
- [6] Xiaoqian Liu, Sarah Robbins, Xia Wang, Sonika Virk, Karen Schuck, Leticia A. Deveza, Win Min Oo, Kirsty Carmichael, Benny Antony, Felix Eckstein, Wolfgang Wirth, Christopher Little, James Linklater, Anthony Harris, David Humphries, R O'Connell, Gillian Heller, Thomas Buttel, Stefan Lohmander, Changhai Ding, and David J. Hunter. Efficacy and cost-effectiveness of stem cell injections for symptomatic relief and structural improvement in people with tibiofemoral knee osteoarthritis: Protocol for a randomised placebo-controlled trial (the sculptor trial). *BMJ Open*, 11(11):e056382, 2021.
- [7] Brendon Wahlberg, Harmanvir Ghuman, Jessie R. Liu, and Michel Modo. Ex vivo biomechanical characterization of syringe-needle ejections for intracerebral cell delivery. *Scientific Reports*, 8, 2018.
- [8] B.A. Aguado, W. Mulyasasmita, J. Su, K.J. Lampe, and S.C. Heilshorn. Improving viability of stem cells during syringe needle flow through the design of hydrogel cell carriers. *Tissue Engineering Part A*, 18(7-8):806–815, 2012.
- [9] G. Morgan, L. Elsawah, A. Esclamado-Cadenas, A. Daudet, J. Frattolin, D. Watson, Q. Xu, N. Neigrini, A. Celiz, and J.E. Jr. Moore. Excessive shear rate, not shear stress, is responsible for cell mechanolysis in small bore needle injections. In *Summer Biomechanics, Bioengineering and Biotransport Conference (SB3C2023)*, 2023.
- [10] H. Lopez Hernandez et al. Non-newtonian polymer-nanoparticle hydrogels enhance cell viability during injection. *Macromolecular Bioscience*, 19(1):1800275, 2018.
- [11] James Moore. Injection device for injection of biological materials. U.S. Patent Application US20240286125A1, 2024. Published by the United States Patent and Trademark Office.
- [12] Inês Miranda, Andrews Souza, Paulo Sousa, João Ribeiro, Elisabete M. S. Castanheira, Rui Lima, and Graça Minas. Properties and applications of pdms for biomedical engineering: A review. *J Funct Biomater*, 13(1):2, 2022.
- [13] Rui Lima, Shigeo Wada, Shuji Tanaka, Motohiro Takeda, Takuji Ishikawa, Ken-ichi Tsubota, Yohsuke Imai, and Takami Yamaguchi. In vitro blood flow in a rectangular pdms microchannel: experimental observations using a confocal micro-piv system. *Biomedical Microdevices*, 10(2):153–167, 2008.
- [14] Álvaro Sánchez-Ferro, M. Elshehabi, C. Godinho, D. Salkovic, M. A. Hobert, J. Domingos, E. Maetzler, W. Maetzler, J. A. Ferreira, B. R. Bloem, and W. Maetzler. New methods for the assessment of parkinson's disease (2005 to 2015): a systematic review. *Movement Disorders*, 31(9):1283–1292, 2016.
- [15] F. Delplace. Laminar flow of newtonian liquids in ducts of rectangular cross-section: an interesting model for both physics and mathematics. *International Journal of Theoretical and Mathematical Physics*, 8(2):52–55, 2018.
- [16] The MathWorks, Inc. *gradient (MATLAB function)*. The MathWorks, Inc., Natick, Massachusetts, 2024. Accessed: 2025-04-10.
- [17] Matthias Köfferlein. Klayout - layout viewer and editor. <https://github.com/KLayout/klayout>, 2025. Accessed: 2025-04-13.
- [18] Ratul Paul, Yuwen Zhao, Declan Coster, Xiaochen Qin, Khayrul Islam, Yue Wu, and Yaling Liu. Rapid prototyping of high-resolution large format microfluidic device through maskless image guided in-situ photopolymerization. *Nature Communications*, 14:4520, 2023.

- [19] J. C. McDonald, D. C. Duffy, J. R. Anderson, D. T. Chiu, H. Wu, O. J. Schueller, and G. M. Whitesides. Fabrication of microfluidic systems in poly(“dimethylsiloxane”). *Electrophoresis*, 21(1):27–40, 2000.
- [20] Thermo Fisher Scientific. Invitrogen human umbilical vein endothelial cells (huvecs). https://assets.thermofisher.com/TFS-Assets/LSG/manuals/MAN0001620_HUVEC_PI.pdf, 2021. Accessed: 2025-04-05.
- [21] Sunayana Chandel, R. Kumaragurubaran, Harsh Giri, and Megha Dixit. Isolation and culture of human umbilical vein endothelial cells (huvecs). In Binu Tharakan, editor, *Vascular Hyperpermeability*, volume 2711 of *Methods in Molecular Biology*. Humana, New York, NY, 2024.
- [22] Thermo Fisher Scientific. Aseptic techniques and safety in cell culture. Accessed: 2025-04-07.
- [23] Manish P. Bhatt, Youngmin Lee, Seungwon Jung, Yong Hyun Kim, Ji Young Hwang, Eunju Han, Woo Seok Park, Seok Hong, Young Kim, and Kunsang Ha. C-peptide protects against hyperglycemic memory and vascular endothelial cell apoptosis. *Journal of Endocrinology*, 231(1):97–108, 2016. Retrieved Apr 10, 2025.
- [24] B. Baudin, A. Bruneel, N. Bosselut, and M. Vaubourdolle. A protocol for isolation and culture of human umbilical vein endothelial cells. *Nature Protocols*, 2(3):481–485, 2007.
- [25] Thermo Fisher Scientific. LIVE/DEAD Viability/Cytotoxicity Kit for Mammalian Cells Protocol. Accessed: 2025-04-04.
- [26] Sandra Sanfilippo, Michel Canis, Lahoucine Ouchchane, Roland Botchorishvili, Caroline Artonne, Luc Janny, and François Brugnon. Viability assessment of fresh and frozen/thawed isolated human follicles: reliability of two methods (trypan blue and calcein am/ethidium homodimer-1). *Journal of Assisted Reproduction and Genetics*, 28(12):1151–1156, Dec 2011.
- [27] L. Fischer, M. Nosratlo, K. Hast, E. Karakaya, N. Ströhlein, T. U. Esser, R. Gerum, S. Richter, F. B. Engel, R. Detsch, B. Fabry, and I. Thievessen. Calcium supplementation of bioinks reduces shear stress-induced cell damage during bioprinting. *Biofabrication*, 14(4):045005, 2022. Accessed: 2025-04-10.
- [28] Abcam. Calcein am staining: A guide, n.d. Accessed: 2025-04-10.
- [29] Thermo Fisher Scientific. *LIVE/DEAD Viability/Cytotoxicity Kit for Mammalian Cells Manual*, n.d. Accessed: 2025-04-10.
- [30] Sang Gyu Kwak and Jong Hae Kim. Central limit theorem: the cornerstone of modern statistics. *Korean Journal of Anesthesiology*, 70(2):144–156, 2017.
- [31] Paul Yager. Basic concepts in microfluidics. <https://faculty.washington.edu/yagerp/microfluidicstutorial/basicconcepts/basicconcepts.htm>, n.d. Accessed: 2025-04-10.
- [32] Yuval Elani. Construction of membrane-bound artificial cells using microfluidics: a new frontier in bottom-up synthetic biology. *Biochemical Society Transactions*, 44(3):723–730, 2016.
- [33] John Saliba, Arij Daou, Samar Damiati, Jessica Saliba, Marwan El-Sabban, and Rami Mhanna. Development of microplatforms to mimic the in vivo architecture of cns and pns physiology and their diseases. *Genes*, 9(6):285, 2018.
- [34] Gunnar Liminga, Petra Martinsson, Bertil Jansson, Peter Nygren, and Rolf Larsson. Apoptosis induced by calcein acetoxyethyl ester in the human histiocytic lymphoma cell line u-937 gtb. *Biochemical Pharmacology*, 60(12):1751–1759, 2000. Retrieved Apr 10, 2025.
- [35] M. C. McNamara, L. Wroblewska, D. Zurakowski, R. Duran-Struuck, M. Ryan, H. Wakimoto, R. Jaenisch, X. O. Breakefield, K. Shah, and D. Irinima. Cells under stress: An inertial-shear microfluidic determination of cell deformability. *Bioophysical Journal*, 116(7):1223–1235, 2019. Accessed: 2025-04-12.
- [36] B. D. Plourde, J. R. Stark, and J. P. Abraham. A new catheter technology to deliver vascular stem-cells. *Studies on Stem Cells Research Therapy*, 2(1):007–016, 2016. Accessed: 2025-04-05.
- [37] A. Prasanphanich, R. Chinnadurai, J. Galipeau, and J. Prologo. Influence of shear stress on trans-catheter stem cell delivery quality. In *Scientific Sessions, JVIRS12*. Emory University, Emory University School of Medicine, 2021. Abstract No. 19, presented at the Sunday Scientific Session.

Appendix

A. Project Management

A.1. Departures from Project Plan

Several setbacks occurred during the execution of the project, leading to deviations from the original plan.

Foremost among these was the death of the initial batch of cultured HUVECs due to the use of M199 cell media (a cheaper alternative), leading to a considerable delay while new cells were cultured and media delivered. Additionally, a lack of available Ethidium Homodimer-1 / Calcein AM assay resulted in a short delay while the necessary reagents were ordered.

Unfamiliarity with the microfabrication process and associated software led to an initial slow start, with the first two wafers produced being unusable. These issues were quickly resolved after several days of troubleshooting.

Minor setbacks also occurred during the cell imaging process. Defects such as bubbles and PDMS debris in the device led to some imaging sessions returning unproductive results. Additionally, various imaging difficulties resulted in iterative design changes that deviated from the version presented in the original project pitch.

To compensate for the delays, we dedicated significant effort to collecting additional data during the holiday period and increasing the number of experimental runs, which enabled us to complete the project successfully.

A.2. Project Planning Lessons

1. Establishing comprehensive contingency plans is essential for effectively navigating both anticipated and unforeseen challenges

We encountered multiple setbacks throughout the duration of the project, which presented themselves in all areas, prompting us to address the importance of anticipating challenges during a biological project. These disruptions underscored the necessity of implementing layered contingency measures: maintaining backup wafer batches, validating staining protocols in advance, and establishing multiple culture flasks. When progressing through the project, developing robust contingency protocols allowed us to ensure that project delays were mitigated to our best ability, while simultaneously maintaining project momentum.

2. Delegating clearly defined responsibilities within sub-teams ensures maximal efficiency on experiment days

From the onset of our project, it was clear to us that the nature of our project required multiple sub-teams because we had several complex tasks to collate for experiments. By splitting into these sub teams, we were able to clearly define responsibilities and ensure members were able to develop their expertise, maximising the learning from this process. Furthermore, by delegating tasks to each group, efficiency was streamlined, delays were reduced, and every member was able to contribute to the broader goals of the project. Most importantly, by implementing this parallel process, experiment days were structured to maximise efficiency during experiment runs.

3. Maintaining flexibility in planning when working on a biological project is vital when managing shared resources and changing project requirements

While a well-defined project plan is necessary for structure and direction, maintaining flexibility is essential when managing complex projects. With our project in particular, the biological nature led to several unexpected challenges which were reliant on shared resources and equipment. Planning for experiments early also helped identify bottlenecks early such as delay in materials and enabled us to reassign tasks or adjust priorities accordingly. Regular weekly meetings with our supervisor allowed us to maintain momentum and allowed us to adapt our project direction. This approach helped manage expectations, ensured steady progress, and helped avoid last minute pressures, leading us to a more successful project outcome.

B. Statistical Methods

The test statistic t is calculated based on the difference between two sample means \bar{X}_1 and \bar{X}_2 , the sample sizes n_1, n_2 , and the sample variances s_1^2, s_2^2 . The two-sample unpaired t-test equation is:

$$t = \frac{\bar{X}_1 - \bar{X}_2}{\sqrt{\frac{s_1^2}{n_1} + \frac{s_2^2}{n_2}}} \quad (6)$$

The degrees of freedom are calculated using Welch's approximation:

$$\nu = \frac{\left(s_{\bar{X}_1}^2 + s_{\bar{X}_2}^2 \right)^2}{\frac{s_{\bar{X}_1}^4}{n_1-1} + \frac{s_{\bar{X}_2}^4}{n_2-1}} \quad (7)$$

At a significance level of $\alpha = 0.05$, the critical value is given by:

$$t_{\text{crit}} = t_{1 - \frac{\alpha}{2}, \nu} = F^{-1} \left(1 - \frac{\alpha}{2}, \nu \right) \quad (8)$$

For $|t| \geq t_{\text{crit}}$, the null hypothesis is rejected, indicating a statistically significant difference.

C. Code Availability

Here is [a link](#) to our GitHub repository containing the code we used to calculate the flow conditions, as well as to perform the statistical analysis and generate the plots for this report.

D. Ethical Considerations

All HUVECs used were sourced commercially under appropriate ethical guidelines, including donor consent. No ethical issues arose from the subsequent experimental work.

E. Acknowledgments

We would like to express our sincere gratitude to all those who contributed to this project.

We thank our supervisor, Professor James Moore Jr., for his invaluable guidance and support throughout the research process.

We also extend our appreciation to Dr. Daniel Watson for his advice and expertise, as well as to Raphael Delattre for his assistance despite other commitments.

Finally, we acknowledge the researchers whose work laid the foundation for our study. Their contributions were instrumental in shaping our understanding.